Microbial Ecosystem Therapeutics 4 (MET4) elicits treatment-specific IgG responses associated with changes in gut microbiota in immune checkpoint inhibitor recipients with advanced solid tumors

Matthew K Wong ,[1] Giselle M Boukhaled,[2] Eric Armstrong,[3] Rachel Liu,[4] Alya A Heirali,[3] Noelle R Yee,[3] Jinny Tsang,[1] Pavlina Spiliopoulou,[5,6] Pierre H H Schneeberger,[7,8] Ben X Wang,[2] Kyla Cochrane,[9] Keith Sherriff,[10] Emma Allen-Vercoe,[9] Lillian L Siu,[2,11] Anna Spreafico ,[2,11] Bryan Coburn[1,3,12]

Correspondence to
Dr Bryan Coburn;
bryan.coburn@uhn.ca

ABSTRACT

Background Gut microbiome modulation has shown promise in its potential to treat cancer in combination with immunotherapy. Mechanistically, the pathways and routes by which gut microbiota may influence systemic and antitumor immunity remain uncertain. Here, we used blood and stool samples from Microbial Ecosystem Therapeutic 4 (MET4)-IO, an early-phase trial testing the safety and engraftment of the MET4 bacterial consortium in immune checkpoint inhibitor recipients, to assess how MET4 may affect systemic immunity.

Methods Circulating antibody responses induced by MET4 were assessed using an antimicrobial antibody flow cytometry assay on pretreatment and post-treatment plasma. Antibody responses were associated with taxonomic changes in stool identified by metagenomic sequencing. Mass cytometry was performed on peripheral blood mononuclear cells to identify shifts in circulating immune subsets associated with antibody responses.

Results Increases in circulating anti-MET4 immunoglobulin G (IgG) responses were measured by flow cytometry post-consortium treatment in MET4 recipients, but not untreated control participants, with five individuals displaying notably higher antibody responses. Stronger IgG responses were associated with greater increases in multiple taxa, including MET4 microbe *Collinsella aerofaciens*, which was previously linked with immune checkpoint response. However, these taxa were not enriched in the IgG-bound fraction post-MET4 treatment. Greater increases in circulating B cells and FoxP3+ CD4+ T cells post-MET4 treatment were observed in the blood of high IgG responders, while CD14+ and CD16+ monocyte populations were decreased in these individuals.

Conclusion These results demonstrate the induction of treatment-specific circulating humoral immunity by a bacterial consortium and suggest potential mechanisms by which gut microbes may contribute to antitumor immunity.

WHAT IS ALREADY KNOWN ON THIS TOPIC

⇒ Microbial interventions have seen success in combination therapy with immune checkpoint inhibitors. Developing ways to determine the efficacy and mechanism of microbe-targeting therapeutics will be crucial in optimizing the design of these therapies.

WHAT THIS STUDY ADDS

⇒ We identified anti-consortium immunoglobulin G (IgG) responses against the Microbial Ecosystem Therapeutic 4 (MET4) bacterial consortium using an antimicrobial antibody assay previously used to identify similar responses in an immunotherapy cohort who received fecal microbiota transplant. High IgG response was associated with changes in the relative abundance of specific MET4 microbes and shifts in circulating immune subsets.

HOW THIS STUDY MIGHT AFFECT RESEARCH, PRACTICE OR POLICY

⇒ This study highlights the immunostimulatory potential of a bacterial consortium in an immunotherapy-treated cancer cohort. Development and evaluation of bacterial consortia or other microbial therapeutics can be informed by using similar assays to identify microbes that may drive systemic immune responses.

INTRODUCTION

The success of immune checkpoint inhibitor (ICI) therapy has improved survival outcomes for many individuals with cancer. Nevertheless, lack of therapeutic response remains an issue for many cancer types. Combination therapy with other interventions, including chemotherapy and radiotherapy,

has augmented therapeutic efficacy of ICI in some cases. Recently, there has been an increased interest in combining ICIs with microbial interventions in clinical trials. Prebiotics, probiotics, fecal microbiota transplants (FMT), and bacterial consortia represent some of the different treatment modalities developed to enhance therapeutic responses.[1–8]

Compared with FMT, bacterial consortia represent a safer, more reproducible, and more stable intervention that maintains the beneficial provision of a diverse community conferred by FMT.[9] Microbial Ecosystem Therapeutic 4 (MET4) is a first-in-class novel microbial therapeutic consisting of an orally delivered consortium of 30 cultivated gut bacterial species derived from healthy donor stool. MET4 was developed for combination therapy with ICIs,[7] with several microbes in this community selected based on their increased abundance in ICI responders.[10–13] An early-phase clinical trial, MET4-IO, tested the safety, tolerability, and engraftment of MET4 concurrent with ICI treatment in participants with advanced solid tumors.[7] MET4 was determined to be safe and tolerable when coadministered with ICI while displaying increases in MET4 taxa in about one-third of participants receiving the consortium.

A recent study evaluating the use of ICI-responder FMT in ICI-refractory individuals observed increased circulating antidonor microbiota immunoglobulin G (IgG) in those who displayed improved therapeutic outcomes following FMT.[4] These findings suggest that these bacterial-specific antibody responses may act as a surrogate marker for antitumor immunity, demonstrating an avenue by which the efficacy of a microbial intervention in enhancing therapeutic responses may be assessed. We sought to use a similar strategy to identify whether anti-consortium antibody responses would similarly be induced by MET4.

We performed antimicrobial antibody flow cytometry on plasma-incubated MET4 to identify circulating antibody responses generated against the consortium. Paired stool metagenomic sequencing was conducted in tandem to uncover potential taxonomic drivers of these systemic immune responses. Additionally, circulating immune subsets in the blood were assessed by mass cytometry for associated changes in circulating immunity post-MET4.

METHODS

### MET4-IO study and collection time points

Individuals with solid tumors were enrolled into MET4-IO, a clinical study that assessed the safety, tolerability, and engraftment of MET4. Out of three cohorts in this study, all samples were taken from "cohort B", which consisted of ICI-naïve participants (n=30) stratified into MET4+ICI or ICI alone controls (figure 1A). From this cohort, 23 participants with paired stool and blood collected pre-MET4 and post-MET4 therapy were included in analyses. Further details of the trial and MET4 consortium have been described previously.[7]

Paired plasma, peripheral blood mononuclear cells (PBMCs), and stool were collected from participants and stored at −80°C (figure 1B). Sample time points used for all analyses were 3–4 weeks into ICI therapy but prior to MET4 (baseline/T0) and 3–4 weeks after initiation of MET4 (window+2 weeks, T2); end of therapy samples were used when T2 was unavailable and if collected proximal to T2 (±2 weeks). Plasma and stool samples were collected within 30 days of each other except for two individuals, who were excluded in paired plasma–stool analysis. PBMCs were also collected from a pretherapy screening time point (pre-ICI, pre-MET4) and included in mass cytometry analysis. Ecological engraftment was determined based on the number of MET4 taxa exhibiting a log-fold increase in post-MET4 relative abundance (RA). Participants with >5 MET4 taxa with one log-fold increase were classified as "engrafters", and those ≤5 were "non-engrafters".

MET4 production and anti-MET4 Ig flow cytometry

30 bacterial species were cultured individually, lyophilized, and combined to form the MET4 bacterial consortium. RA of constituents differed depending on the taxon. The drug product was assessed for consistency based on detection of MET4 strains, bacterial count variability (<20% for each genus), contamination at the genus level, and sufficient colony-forming units (CFU)/capsule across batches. MET4 was anaerobically resuspended in 10 mL of phosphate-buffered saline (PBS) degassed in an anaerobic chamber overnight, washed, and approximately 1.4×10^8 cells were stained with 5 µM carboxyfluorescein succinimidyl ester (CFSE) (Cell-Trace, Invitrogen) for 30 min at 37°C under anaerobic conditions. During the stain, a 1:200 plasma dilution was prepared in staining buffer (PBS+2% bovine serum albumin (BSA) + 2 mM EDTA) for each sample time point. Diluted plasma was incubated at 56°C for 30 min to inactivate complement. Inactivated plasma was centrifuged at 10,000 RPM for 10 min at 4°C to remove antibody complexes. Supernatant was kept and serially diluted 1:2 three additional times in staining buffer (1:200–1:1600, four dilutions total).

MET4 was diluted in staining buffer to 2×10^6 cells/100 µL following CFSE stain. Diluted MET4 was incubated with each plasma dilution in a 1:1 ratio (50 µL to 50 µL, 1×10^6 bacteria total) for 30 min at 4°C. Secondary staining with goat anti-IgA AF647 (1:100, cat#2052–31) and anti-IgG PE (1:200, cat#2042–09) Fab fragments (polyclonal, SouthernBiotech) for 30 min at 4°C was performed. All staining steps were followed by two washes with staining buffer and all centrifugation steps were performed at 4000 × g. Samples were fixed for 30 min with 4% paraformaldehyde and kept at 4°C in the dark until acquisition on a BD LSRFortessa. Analysis was performed on FlowJo V.10.9.0 (BD). Figures were generated in GraphPad Prism V.10 (GraphPad Software).
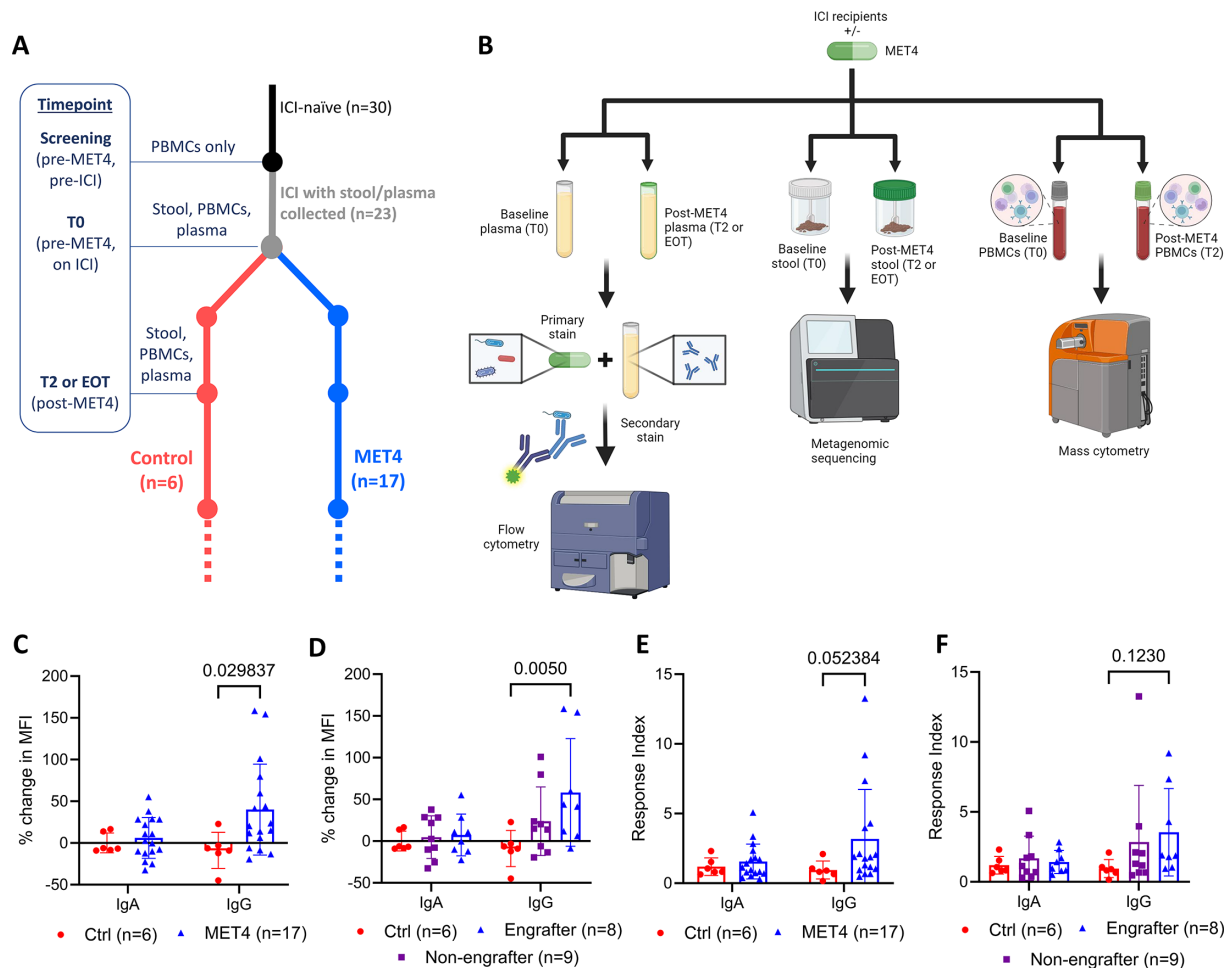
Figure 1 Increased IgG responses induced in participants receiving MET4. (A) Timeline describing sample time points for treatment and control arms from the MET4-IO cohort B. Time points where samples are collected are labeled. Stool and plasma were collected at T0 and T2/EOT, while peripheral blood mononuclear cells (PBMCs) were collected at all labeled time points. T0=3–4 weeks into ICI therapy, pre-MET4; T2=3–4 weeks after MET4 initiation; EOT=end of therapy (used when T2 unavailable and if±2 weeks from T2). (B) Flow chart depicting samples collected and preparation of each assay. (C–F) Anti-MET4 immunoglobulin (Ig) flow cytometry was performed using fluorophore-conjugated anti-Ig secondary antibodies against MET4-IO participant plasma incubated with MET4 microbes. Percent change in Ig geometric mean fluorescent intensity (MFI) post-MET4 treatment at 1:200 plasma dilution (C–D) and Ig response index (E–F) stratified by MET4 treatment (C,E) or engraftment (D,F). Mann-Whitney or Tukey's multiple comparisons tests following 2-way ANOVA were performed for (C–F). Flow chart (B) was created on biorender.com. ANOVA, analysis of variance; ICI, immune checkpoint inhibitor; MET4, Microbial Ecosystem Therapeutic 4.

Response index calculation

Calculations were performed with modification from a previously described method.[14] Frequency and geometric mean fluorescence intensity (MFI) were collected for IgA and IgG at each time point. MFIs from each plasma serial dilution were log2 transformed, linearly plotted, and area under the curve (AUC) was calculated. The response index (RI) was calculated as the 2-fold change in AUCs using the difference of post-treatment and baseline: $2^{(\text{Post-MET4 Ig MFI AUC} - \text{Baseline Ig MFI AUC})}$. Individuals with IgG RI greater than 3 were classified as "high response index", while those with less than 3 were classified as "low response index".

Immunoglobulin ELISA

Antibody concentration was measured using IgA and IgG (total) Human ELISA kits (Invitrogen). Briefly, plasma

was diluted as recommended by the kit protocol (1:10 000 and 1:500 000 for IgA and IgG, respectively). Plasma was added to Ig-coated ELISA plates and incubated at room temperature. Samples were subsequently incubated with anti-Ig secondary conjugated to horseradish peroxidase (HRP). 3,3′,5,5′-tetramethylbenzidine (TMB) substrate was added for about 10 min before stopping the reaction with 2N sulfuric acid. Absorbance was measured at 450 nm using a Tecan microplate reader.

Metagenomic sequencing of human stools

Paired stools (baseline and post-MET4) were thawed and transferred into an anaerobic chamber for processing. 1–3 g of stool was weighed and resuspended in overnight degassed PBS+20% glycerol at a ratio of 10 mL/g of stool. Resuspended stool was filtered through a 300 µm Whirl-Pak filter bag (Nasco) to remove stool particulates.

Stool slurries were frozen at −80°C until DNA extraction. Qiagen's DNeasy PowerSoil Pro kit was used to extract DNA from 300 µL of stool slurries. Purified DNA was quantified using a Qubit fluorometer (Invitrogen). Samples were normalized to 300 ng or the highest possible quantity for input into Illumina's DNA Prep library preparation kit. Nextera 96-well CD indexes (Illumina) were used for post-tagmentation indexing. Libraries were normalized, pooled, and sequenced on an Illumina MiniSeq with a MiniSeq High Output Reagent Kit (Illumina) to obtain approximately 500,000 reads per sample (25 million reads in total).

Sequence data processing
Sequence quality was assessed with FastQC V.0.11.9.[15] Since quality was high, no sequence trimming was performed. Nextera adapters were trimmed with Trimmomatic V.0.39.[16] Human, phiX, and mouse reads were removed with KneadData V.0.7.2.[17] Taxa were identified from cleaned reads using MetaPhlAn V.4.0.6 using default settings and database vOct2022.[18 19]

IgG cell sorting
MET4 and plasma samples from 11 individuals (8 MET4-treated, 3 control) were prepared using the staining protocol described above at a 1:200 plasma dilution. Bacterial cells were sorted on a BD FACSymphony S6 SE (BD Biosciences) for IgG-bound and IgG-unbound populations, with 5×10^5–1×10^6 cells collected for both populations in PBS.

16S quantitative PCR
DNA was extracted from IgG-sorted samples using Qiagen's DNeasy Powersoil Pro kit. Quantitative PCR (qPCR) was performed on DNA using primers against taxa-specific 16S and groEL taken from other studies (online supplemental table 1).[20–24] Retention of MET4 microbes throughout staining and cytometer processing were assessed and reported in online supplemental figure 1 A–B.

16S rRNA sequencing
IgG-sorted DNA was submitted for 16S ribosomal RNA sequencing to the Centre for the Analysis of Genome Evolution and Function. The V4 hypervariable region of the 16S ribosomal RNA gene was amplified using uniquely barcoded 515F (forward) and 806R (reverse) sequencing primers to allow for multiplexing.[25] Amplification reactions were performed using KAPA2G Robust HotStart ReadyMix (Kapa Biosystems) and required primers. Amplification steps were 95°C/3 min, 18× cycles (for MET4) or 28× (for cell sorted samples) of 95°C/15 secs, 50°C/15 secs and 72°C/15 secs, followed by a 5 min 72°C extension. All amplification reactions were done in duplicate, pooled, and checked on a 1% agarose TBE gel. Pooled duplicates were quantified using PicoGreen and combined by even concentrations. The library was purified using Ampure XP beads and sequenced on an Illumina MiSeq according to manufacturer instructions using

V2 (150 bp × 2) chemistry. A single-species (*Pseudomonas aeruginosa* DNA), a mock community (Zymo Microbial Community DNA Standard D6305), and a template-free negative control were included.

Processing of 16S sequencing data
The QIIME2 analysis package V.2024.5 was used for sequence analysis.[26] Quality was examined using FastQC and MultiQC.[15 27] Cutadapt was used following default settings to remove sequences with high error rates.[28] Paired-end sequences were assembled and quality trimmed using vsearch –fastq_mergepairs[29 30] following default settings with –fastq_truncqual set at 2, maxee set at 1, and minimum/maximum assemble lengths set at 250 and 255 (+2 and −3 base pairs from expected sequence length of 253 bp). Assembled sequences were additionally filtered using the quality-filter function and processed following the deblur pipeline. Sequences were clustered into amplicon sequence variant (ASV) groups and singleton sequences were removed. The taxonomy assignment was executed using the classify-hybrid-vsearch-sklearn function and the Average ReadyToWear trained Silva database V.138.1.[31 32] ASVs with an abundance less than 0.01% or identified as contaminating chloroplast or mitochondria were removed. A phylogenetic tree was created using the SATé-enabled phylogenetic placement (SEPP) function in QIIME2.[33]

Microbiome analysis
For stool metagenomic sequencing, taxonomic tables were filtered by removing taxa contributing less than 0.1% RA in one sample. Sequenced MET4 was used as reference for MET4 taxa lists used in this study; known composition of MET4[7] and taxonomic annotations used for analysis are listed in online supplemental table 2. For IgG-sorted samples, the decontam package V.1.24.0[34] was used to eliminate contaminants based on prevalence in negative samples. Taxonomic tables were filtered by removing taxa less than 0.1% of total sequenced abundance; some low abundance MET4 taxa were added back in based on known composition.[7]

QIIME2 was used to generate alpha diversity analysis. The MaAsLin2 package V.1.7.3[35] was used to identify taxa associated with IgG AUC or RI for stool sequencing, or identify taxa enriched at the post-MET4 time point for IgG-sorted samples. For each model, the fixed effect was either IgG AUC at both visits or RI and taxa were represented by either RAs or change in RA from T0 to T2. For models that included repeated measurements from individual participants, participant ID was included as a random effect. Default MaAsLin2 analysis parameters were used, and the false discovery rate was used to control for multiple comparisons. A q value of 0.05 was considered significant.

Mass cytometry immunostaining and analysis
Staining for mass cytometry was performed as described.[36] Briefly, after PBMCs were thawed and washed with PBS,

cells were resuspended in 1 uM Cell-ID Intercalator 103Rh with anti-CD45 conjugated to either 194Pt or 198Pt. Cells were incubated for 15 min at 37°C, washed, and fixed with eBioscience Foxp3 fixation buffer (Thermo Fisher). Following fixation, cells were washed with 1× Barcoding Perm Buffer (Standard BioTools) and incubated for 30 min at room temperature with a unique palladium barcode (Cell-ID 20-plex barcoding kit, Standard BioTools). After barcoding, samples were washed several times in cell staining media and pooled into a single tube. Pooled cells were resuspended in Fc blocking reagent for 10 min followed by addition of a cocktail of surface antibodies prepared in PBS+2% fetal bovine serum. Cells were incubated for 30 min at 4°C, washed, and subsequently stained with a cocktail of intracellular antibodies prepared in 1× Perm wash buffer (Thermo Fisher) for 30 min at 4°C. Finally, cells were incubated with 125 uM Cell-ID Intercalator-Ir for 1 hour at 4°C and were stored in PBS+1.6% paraformaldehyde until acquisition.

Samples were acquired on a Helios instrument (Standard BioTools) and normalized flow cytometry standard (FCS) files were manually de-barcoded in FlowJo V.10.8.1 software (BD Biosciences). Gates were applied to remove beads, doublets, ion fusions and dead cells, finally gating on total CD45$^+$ events. CD45$^+$ single-cell intensities were imported into R for transformation and high-dimensional analysis. A custom scaling factor was used for each channel during hyperbolic arcsine transformation to account for different background intensities of certain antibodies. Dimensionality reduction was performed using the package umap (V.0.2.7.0) in R (V.4.0.0) with the "umap-learn" method. Clustering using a subset of lineage-determining markers was performed using the fast-Phenograph algorithm using the Fast-PG package (V.0.0.6) in R (V.3.6.2). Remaining analyses were performed in R (V.4.2.1). Clusters were manually annotated based on lineage marker expression to denote the immune population. Differential abundance analysis was performed using the "edgeR" test from the diffcyt package (V.1.16.0). Visualizations were generated using functions from ggplot2 (V.3.4.0), pheatmap (V.1.0.12), ggh4x (V.0.2.3), and ggpubr (V.0.4.0) packages.

RESULTS
MET4-specific circulating IgG responses are elevated in MET4 recipients

To investigate possible treatment-specific antibody responses induced by MET4, plasma, PBMCs, and stool were collected before and after MET4 treatment from participants of cohort B in MET4-IO (figure 1A), consisting of ICI-naïve individuals given standard-of-care ICI therapy who were randomized into MET4 or control groups. Plasma was used in an antimicrobial antibody assay measuring plasma IgA and IgG binding to MET4 (figure 1B). Ig-bound MET4 bacteria were detected using flow cytometry (online supplemental figure 2).

Antibody responses were quantified by calculating percent change in Ig geometric MFI, representing differences in Ig binding intensity post-MET4, and change in percent IgG bound, which corresponds to differences in frequency of MET4 taxa bound by IgG after treatment, at the lowest plasma dilution (1:200). Percent change in IgG MFI was elevated in MET4-treated participants and engrafters compared with the control group (figure 1C,D). Change in percent IgG bound to MET4 showed a similar increase in these same groups (online supplemental figure 3 A and B), while no differences in IgA binding were observed for any of these comparisons. Both IgA and IgG concentrations were similar across groups and time points, indicating increased IgG binding in MET4 recipients was not due to greater plasma antibody density (online supplemental figure 3C).

RI, which measures antibody responses across by comparing differences between time points for AUC of Ig MFI across all plasma dilutions (online supplemental figure 4A–C), was calculated for each pair of plasma samples from participants. RI was also increased in the MET4 and engrafter groups compared with the control (figure 1E,F). A subset of participants (n=5) showed notably higher IgG responses by RI>3 (figure 1E) and were analyzed as a separate group in subsequent analyses. Antibody response metrics were means from three separate runs and participant-level data are shown in online supplemental figure 5.

Clinical outcomes available for each MET4-IO participant were also compared with antibody responses generated following MET4 treatment. When divided into MET4 treatment groups, greater percent change in IgG MFI was observed in MET4 recipients without clinical benefit (progressive disease [PD] by Response Evaluation Criteria in Solid Tumors [RECIST] V.1.1) and ICI non-responders (PD or stable disease [SD]) compared with control participants, although this difference was likely driven by MET4 treatment (online supplemental figure 6 A and B). No differences in anti-MET4 IgG response were observed between participants with RECIST response versus non-response.

MET4 engrafters and IgG responders to MET4 display greater increases in *Bifidobacterium adolescentis* and *Collinsella aerofaciens*

We evaluated ecological and taxonomic changes in cohort B participant stool stratified by ecological engraftment and IgG RI to identify if changes in specific MET4 taxa were associated with these features. Following MET4 treatment, the change in Shannon's Diversity Index was greater in MET4 engrafters compared with controls, and in high IgG RI (>3) participants compared with controls and low IgG RI (<3) (online supplemental figure 7A and B). Greater increases in the RA of individual MET4
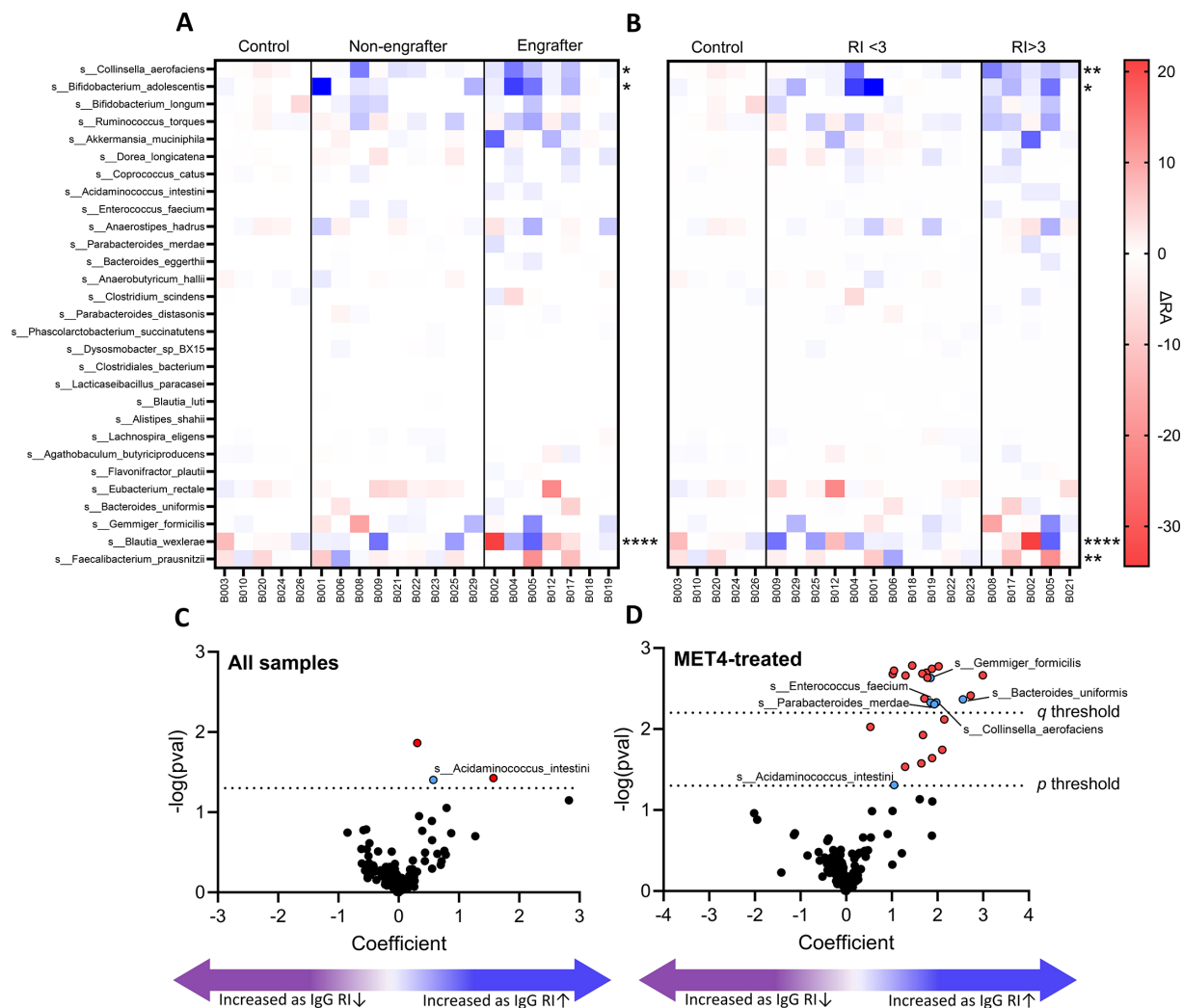
Figure 2 MET4 recipients with high IgG responses display greater increases in some MET4 taxa post-treatment. Paired stools from participants before and after MET4 treatment were collected and sequenced by shotgun metagenomic sequencing using an Illumina MiniSeq. MET4 taxonomic tables were subsequently filtered by removing species less than 0.1% of MET4 relative abundance; some low abundance MET4 taxa were added back in based on known composition. (A–B) Relative abundance difference for individual MET4 taxa depicted by heat maps stratified by (A) engraftment status and (B) response index group. Taxa are ordered by cumulative mean difference from baseline for all groups, while participants are ordered chronologically (A) or by increasing response index (B). Asterisks in the legend highlight the strongest differences among the three groups displayed. Tukey's multiple comparisons test following two-way ANOVA performed for (A–B). *=p<0.05; **=p<0.01; ***=p<0.001. (C–D) Association between response index (RI) and change in relative abundance of taxa from T0 to T2 in (C) all participants and (D) only participants who received MET4. Each dot represents an individual bacterial taxon. Red dots indicate taxa with p<0.05, black dots are non-significant, blue dots indicate MET4 taxa and are labeled. Dotted lines display significance threshold at p=0.05 or q=0.05. P values, q values, and coefficients determined with MaAsLin2. Arrows created with BioRender. ANOVA, analysis of variance; IgG, immunoglobulin G; MET4, Microbial Ecosystem Therapeutic 4.

taxa (online supplemental table 2) were observed in MET4 engrafters and high RI participants compared with their counterparts when assessing only MET4 taxa following MET4 treatment (figure 2A,B). *Bifidobacterium adolescentis* and *Collinsella aerofaciens* RA increased in engrafters compared with controls and in high RI participants compared with controls or low RI (figure 2A,B, online supplemental figure 8A and B). In contrast, *Blautia wexlerae* decreased more in engrafters (figure 2A, online supplemental figure 8A) and high RI participants (figure 2B, online supplemental figure 8B) compared with their counterparts,

while *Faecalibacterium prausnitzii* was decreased in high RI participants compared with low RI and control groups. When analyzing change in overall MET4 abundance between RI groups (online supplemental figure 9A), there was a greater average fold change in MET4 taxa after treatment in the high RI group (online supplemental figure 9B), suggesting that stronger IgG responses were observed with better MET4 engraftment.

Increased anti-MET4 IgG responses are linked with increases in multiple taxa

Commensal gut bacteria can elicit the production of circulating IgG antibodies even at steady state, with various taxa identified as stronger drivers of antibody responses.[37] We assessed general taxonomic drivers of anti-MET4 IgG responses in the MET4-IO cohort by performing a multivariate association with linear models (MaAsLin2) analysis on all taxa identified by sequencing (online supplemental table 3). IgG RI (change in IgG response) and AUC of IgG MFI across plasma dilutions (time point-specific IgG response) were used as continuous or categorical fixed effects. Change in RA was used as the dependent variable for IgG RI to uncover microbes associated with increases in IgG response, while RA was used for IgG AUC to identify taxa associated with IgG response regardless of time point. Covariates controlled for included participant and MET4 administration.

After multiple comparisons correction, increases in continuous IgG RI were not associated with change in RA of any taxa when assessing all participants (figure 2C). However, when analyzing MET4-treated participants, changes in RA of several MET4 taxa were linked with an increase in IgG RI, including MET4 taxa *C. aerofaciens* (coef=1.97), *Enterococcus faecium* (coef=1.84), *Bacteroides uniformis* (coef=2.56), *Parabacteroides merdae* (coef=1.93), and *Gemmiger formicilis* (coef=1.85, figure 2D). Changes in taxa including *Acidaminococcus intestini* were associated with increases in IgG RI prior to correction for multiple comparisons (figure 2D). Similarly, stratifying IgG response into categorical high or low RI resulted in no significant taxa, but RA change in multiple taxa— including *C. aerofaciens* and *B. longum*—was elevated in high RI participants prior to correction (online supplemental figure 10A and B).

When identifying general inducers of the MET4 IgG response across time points, no taxa were enriched as IgG AUC increased postcorrection in all or MET4-treated participants (online supplemental figure 10C and D). However, multiple taxa were enriched before correction as IgG AUC increased in all participants, including *Akkermansia muciniphila* and *Bacteroides eggerthii* (online supplemental figure 10C). For MET4-treated participants, *A. muciniphila* and *Bacteroides eggerthii* were also elevated with increasing IgG AUC before correction, while microbes including *Dorea longicatena* and *F. prausnitzii* were increased in RA with decreasing IgG AUC (online supplemental figure 10D).

Anti-MET4 responses are predominantly increased against IgG bound *Acidaminococcus*
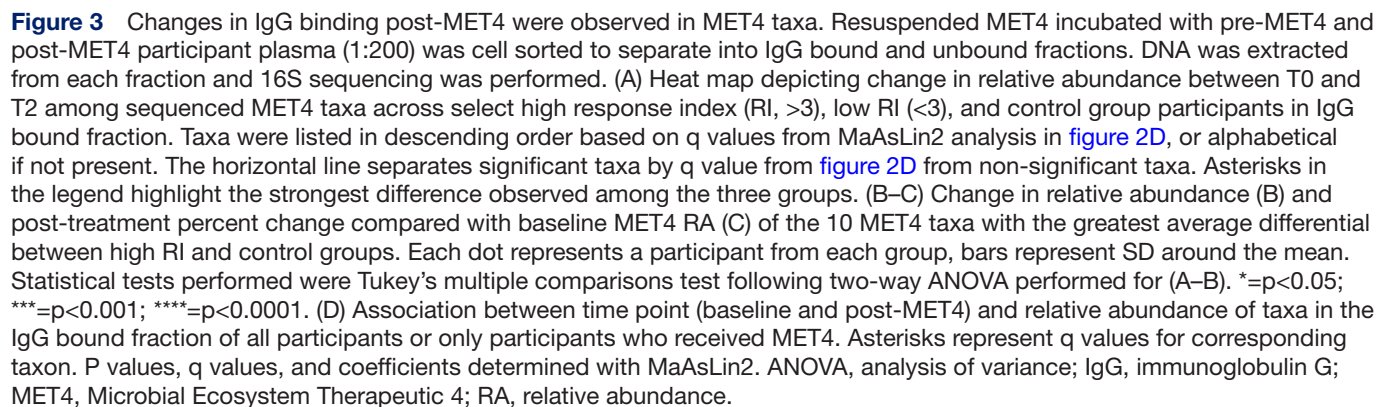
To directly assess which MET4 taxa IgG responses were generated against, IgG-bound and IgG-unbound fractions were separated from plasma-incubated MET4 via cell sorting. DNA was extracted from sorted samples and 16S sequencing was performed to assess the composition of each fraction. In the IgG bound fraction, there were greater increases in the RA of *Acidaminococcus* in high

RI samples compared with low RI and control samples after MET4 therapy, while decreases in the abundance of *Anaerostipes* and *Blautia* were observed in the high RI group compared with controls (figure 3A,B). A decrease in *Acidaminococcus* was noted in high RI samples in the IgG-unbound fraction, while increases in *E. durans* and *B. longum* were seen in high RI samples compared with controls (online supplemental figure 11A and B). Similar trends were seen across both IgG-bound and IgG-unbound fractions when comparing change in percent RA compared with baseline MET4 RA, with additional decreases in *Lactobacillus casei*, *B. longum*, and *Agathobacter* observed in IgG-bound fractions of MET4-treated participants compared with control (figure 3C, online supplemental figure 11C).

MaAsLin2 analysis was also performed to account for the effect of compositionality due to large changes in abundance of *Acidaminococcus* after treatment (online supplemental table 3). RA of the IgG-bound or IgG-unbound fraction was the feature variable, time point (baseline or post-MET4) was the fixed effect, and participant ID was controlled for as a covariate. When assessing all samples, no taxa were elevated postcorrection for multiple comparisons in the bound or unbound fractions (figure 3D, online supplemental figure 11D). *Anaerostipes*, *Blautia*, *Butyricicoccus*, *Dorea*, *C. aerofaciens*, and *P. merdae* were more enriched at baseline precorrection among these samples. However, for MET4-treated individuals, *Anaerostipes*, *Blautia*, *Butyricicoccus*, *C. aerofaciens*, *Lacticaseibacillus* sp, and *P. merdae* were enriched in the bound fraction at baseline postcorrection (figure 3D). In contrast, *Acidaminococcus* was enriched post-MET4 in the bound fraction (coef=0.507, figure 3D), while a corresponding trend in enrichment of *Acidaminococcus* at baseline was noted in the unbound fraction for MET4-treated samples (online supplemental figure 11D).
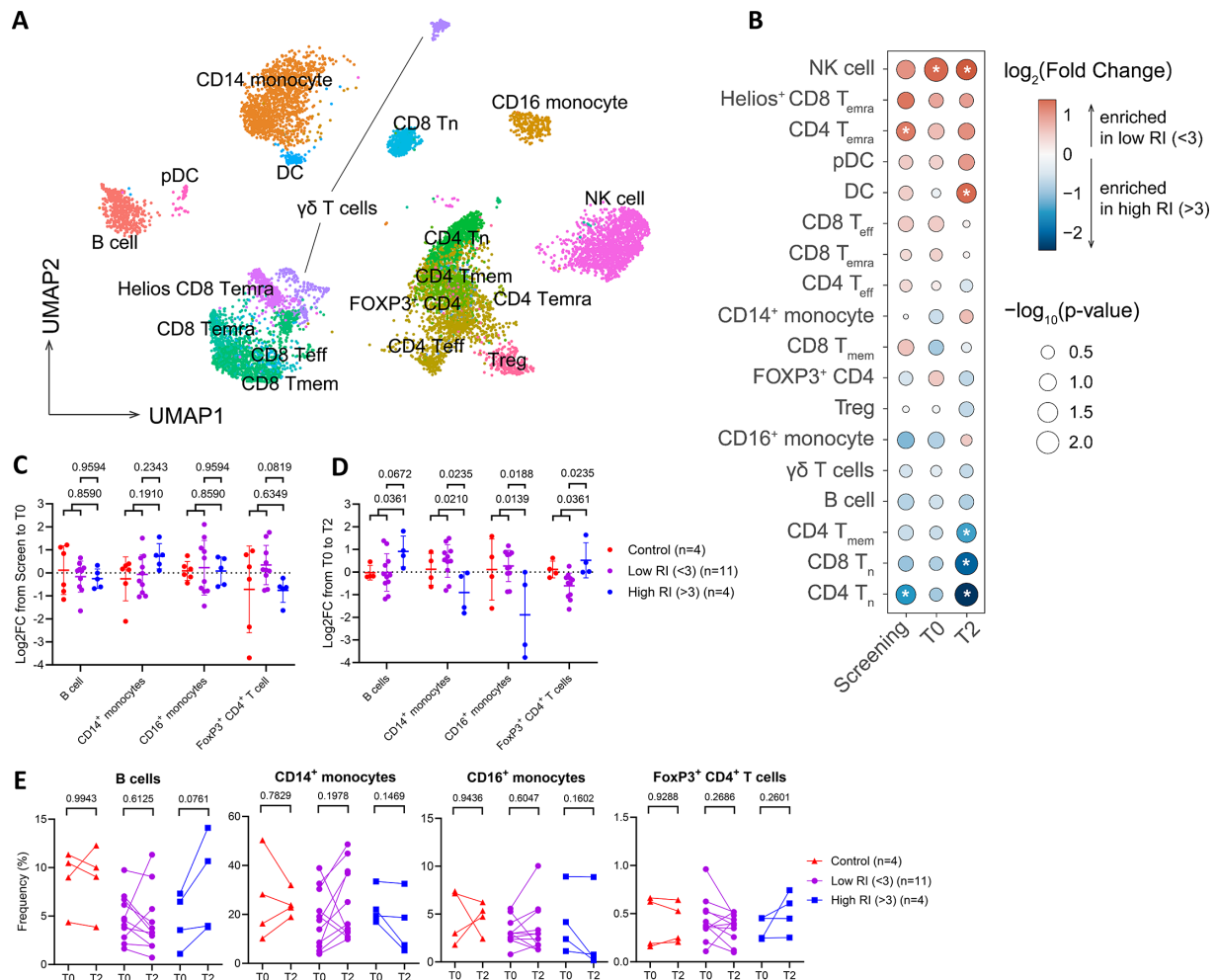
Shifts in B cell and monocyte populations observed at post-MET4, but not pre-MET4, treatment time points in high IgG RI participants

Baseline immune populations and changes induced by MET4 treatment may be correlated with IgG responses observed in our cohort. To investigate the immune profile and how it changes over the course of MET4 therapy, PBMCs were collected at the time of screening, T0 and T2 from cohort B participants (figure 1A) and analyzed by mass cytometry using a panel of 34 metal-tagged antibodies to delineate the majority of immune subsets as well as their activation and functional status (figure 4A). We first assessed whether there were differences in immune profiles of MET4 recipients with high IgG RI compared with low RI (figure 4B, online supplemental figure 12). At screening, naïve CD4+ T cells were enriched in high RI participants whereas CD4+ terminally differentiated effector memory T cells (TEMRA) were enriched in low RI participants. However, this difference was not observed at T0, and instead a greater abundance of natural killer cells was observed in IgG low RI participants compared

Figure 3 Changes in IgG binding post-MET4 were observed in MET4 taxa. Resuspended MET4 incubated with pre-MET4 and post-MET4 participant plasma (1:200) was cell sorted to separate into IgG bound and unbound fractions. DNA was extracted from each fraction and 16S sequencing was performed. (A) Heat map depicting change in relative abundance between T0 and T2 among sequenced MET4 taxa across select high response index (RI, >3), low RI (<3), and control group participants in IgG bound fraction. Taxa were listed in descending order based on q values from MaAsLin2 analysis in figure 2D, or alphabetical if not present. The horizontal line separates significant taxa by q value from figure 2D from non-significant taxa. Asterisks in the legend highlight the strongest difference observed among the three groups. (B–C) Change in relative abundance (B) and post-treatment percent change compared with baseline MET4 RA (C) of the 10 MET4 taxa with the greatest average differential between high RI and control groups. Each dot represents a participant from each group, bars represent SD around the mean. Statistical tests performed were Tukey's multiple comparisons test following two-way ANOVA performed for (A–B). *=p<0.05; ***=p<0.001; ****=p<0.0001. (D) Association between time point (baseline and post-MET4) and relative abundance of taxa in the IgG bound fraction of all participants or only participants who received MET4. Asterisks represent q values for corresponding taxon. P values, q values, and coefficients determined with MaAsLin2. ANOVA, analysis of variance; IgG, immunoglobulin G; MET4, Microbial Ecosystem Therapeutic 4; RA, relative abundance.

with IgG high and was maintained through T2. At T2, IgG high RI participants had a significantly higher frequency of naïve CD4$^+$ and CD8$^+$ T cells, and memory CD4$^+$ T cells.

Since distinct immune populations were differentially abundant at each time point, it is possible that immune composition changed in response to therapy and that these changes were correlated with the ensuing anti-MET4 IgG response. To understand the dynamics of the immune profile post-therapy, we calculated fold change in abundance of each immune population between screening to T0 and between T0 and T2. Any changes that occurred between T0-screening could be

the result of the first dose of ICI while changes between T2 and T0 could be attributed to the initiation of MET4 treatment. Participants with high IgG RI displayed an increase in B cells and FoxP3$^+$ CD4$^+$ T cells and a decrease in CD14$^+$ and CD16$^+$ monocytes by log-fold change post-MET4 treatment compared with individuals with low IgG RI and showed similar shifts when restricted to MET4 recipients with low IgG RI; these changes were not seen prior to MET4 initiation (figure 4C,D). When assessing differences in immune subset frequencies between T0 and T2 for each RI group, B cells in high IgG RI participants tended to increase post-MET4, while low IgG RI

Figure 4 Shifts in immune subsets post-MET4 in high response index group. (A) Uniform Manifold Approximation and Projection (UMAP) clustering of peripheral blood mononuclear cells from MET4-IO participants analyzed by mass cytometry. (B) Log2 fold change (FC, low RI compared with high RI) of immune subsets from peripheral blood mononuclear cells (PBMCs) in MET4 recipients at screening (pre-ICI, pre-MET4), T0 (post-ICI, pre-MET4), and T2 (post-ICI, post-MET4). Red circles indicate enrichment in the low RI group, while blue circles are enriched in the high RI group. The size of the circle indicates significance by p value. (C–D) Log2 fold change of immune subsets from participant screening to T0 (post-ICI, pre-MET4) (C) or T0 to T2 (post-MET4) (D). (E) Difference in subset frequency at T0 versus T2 in high versus low RI and control groups. EOT (end of therapy) samples were not included in these analyses. Statistical tests performed were multiple unpaired t-tests (C–D) and multiple paired t-tests (E) with Holm-Šídák multiple comparisons test. Unadjusted p values are shown for (B, E). DC, dendritic cell; ICI, immune checkpoint inhibitor; MET4, Microbial Ecosystem Therapeutic 4; NK, natural killer; pDC, plasmacytoid dendritic cell; RI, response index.

and control participants showed limited changes across immune subsets (figure 4E).

DISCUSSION

Recent successes in combining microbial interventions with cancer immunotherapy include studies demonstrating the effectiveness of FMT in eliciting therapeutic responses in ICI-refractory[4 5] and treatment-naïve[38 39] individuals. Antidonor FMT IgG responses were found to be a correlate of induced ICI response in one of these studies,[4] and we sought to determine if similar anti-intervention antibody responses were generated in an early-phase trial (MET4-IO) that administered a novel bacterial consortium, MET4, to ICI recipients.[7]

In this study, circulating IgG responses against MET4 were more strongly elicited in MET4 recipients, with a subset of five participants displaying highly elevated IgG responses after MET4 therapy. High IgG responders displayed increased RA of multiple MET4 and endogenous taxa. However, the taxa whose stool abundance was associated with increased IgG responses were not enriched for IgG binding, suggesting that taxa associated with binding were not necessarily those targeted by antibody responses. Individuals with increased IgG responses after treatment also exhibited greater increases in circulating B cells and FoxP3^{+} CD4^{+} T cells and decreases in CD14^{+} and CD16^{+} monocytes than individuals with lower IgG responses, suggesting that the introduction of MET4

microbes led to altered regulation of both lymphoid and myeloid populations in the blood.

Although many taxa were identified as possible MET4-specific IgG inducers, *C. aerofaciens*, *E. faecium*, *P. merdae*, and *G. formicilis* were the primary MET4 microbes associated with increased IgG responses in MET4 recipients. Similarly, there was a greater increase in *C. aerofaciens*, *B. adolescentis*, and *B. longum* RA in high IgG responders. Several of these commensal microbes have previously been associated with ICI response[11 12] or have been shown to induce circulating antibodies following translocation through the gut barrier,[40] suggesting that they may act as strong stimulators of systemic immune responses. This indicates a potential microbiota-mediated link between the development of antitumor ICI responses and circulating humoral immunity, possibly through bacteria acting as an immune adjuvant.

Cancer vaccines have long employed the use of adjuvants to enhance antitumor memory responses generated by vaccine antigens.[41] With gut bacteria, binding of microbial components to pattern recognition receptors can activate antigen-presenting cells to express costimulatory molecules and initiate production of cytokines that can alter antitumor immunity.[42] One example of this interaction was described in a study that identified bacterial peptidoglycan hydrolase SagA to be linked with ICI response via NOD2 activation by SagA-derived muropeptides.[43] Thus, although the circulating IgG responses we observed in this study are not necessarily directly involved in antitumor immunity, they may be indicative of changes in broader systemic immunity. This was exemplified by post-MET4 increases in circulating B cells and FoxP3^{+} CD4^{+} T cells and decreases in CD14^{+} and CD16^{+} monocytes in high IgG responders from this study, with both lymphocyte and monocyte populations being known to respond to microbial signals from the gut.[44 45]

Additionally, this idea of "adjuvant taxa" may also extend to antibody responses generated. Although enrichment of *C. aerofaciens* and *Enterococcus* species was observed with increased IgG response post-MET4, IgG responses appeared to be directed primarily against *Acidaminococcus* despite its limited engraftment. This suggests that engrafting immunostimulatory taxa may be distinct from those against which IgG responses are generated. Instead, engrafting microbes may act as adjuvant taxa triggering increased heterologous antibody responses connected to general activation of systemic and peripheral immunity, which may occur with or without systemic translocation[40] and may be toll-like receptor-dependent.[37]

Proportionally stronger increases in *Acidaminococcus* in the IgG bound fraction may also explain post-treatment decreases in IgG binding for MET4 taxa. That is, large increases in *Acidaminococcus* abundance might lead to a corresponding decrease in RA of other taxa. Investigating the connection between engraftment of microbes, the generation of systemic immunity, and targets of that immunity will be important in understanding how circulating antibody and antitumor responses may be induced by gut microbiota.

This work has the following limitations. As MET4-IO focused primarily on safety and engraftment of MET4, the trial was not sufficiently powered to draw conclusions on therapeutic outcomes and was confounded by multiple tumor types in enrolled individuals. Longer-term outcomes were also not evaluable due to lack of availability of these sample time points for many participants. A more comprehensive longitudinal study focusing on MET4 and immunotherapy responses in a restricted cancer cohort would be required to thoroughly describe the relationship between MET4, induced humoral immunity, and ICI response. Additionally, for stool sample analysis, taxonomic assignment during microbial profiling performed with MetaPhlAn V.4.0.6 may differ from newer versions with updated taxonomy assignment. However, enrichment of known MET4 taxa in the high IgG response group and/or MET4 recipients was observed, indicating any differences in labeling did not strongly affect identification of taxa known to be part of the consortium.

The anticommensal Ig assay has important limitations. First, despite the absence of differences in plasma antibody concentrations between time points at a group level, some individuals had reduced levels of antibodies post-treatment that also displayed strong decreases in Ig responses (data not shown). However, this was only observed in control participants or with IgA responses, neither of which were associated with changes post-treatment. Additionally, the assay was limited in its retention of certain microbes throughout preparation and processing. The presence of MET4 taxa by 16S or groEL qPCR varied by microbe throughout processing steps, while greater overall log-fold decreases than expected were observed post-cell sorting. This may be due to size exclusion during centrifugation or gating, decreased viability of more sensitive microbes (eg, anaerobes), or smaller proportions of specific taxa in the starting material. Thus, antibody responses against some taxa may be masked when using this assay to assess complex microbial communities, such as MET4 or stool. This contributes to increased Type II error, which could be problematic if antibody responses are driven by an excluded microbe. Nevertheless, the presence of a strong anti-MET4 IgG response in multiple participants indicates that the assay was sufficient to identify anti-consortium responses in this study.

Altogether, this study demonstrated the immunostimulatory potential of the MET4 bacterial consortium through the generation of treatment-specific circulating antibody responses associated with increases in ICI response-associated taxa and shifts in circulating immune populations. The gnotobiotic nature of bacterial consortia allows for taxonomic modifications to more effectively induce systemic immunity based on taxa linked with humoral responses. Further development of bacterial consortia using similar assessments of systemic immune stimulation

will be informative for designing optimal microbial communities aimed at augmenting antitumor immunity.

Author affiliations
[1]Department of Immunology, University of Toronto, Toronto, Ontario, Canada
[2]Tumor Immunotherapy Program, Princess Margaret Cancer Centre, University Health Network, Toronto, Ontario, Canada
[3]Toronto General Hospital Research Institute, University Health Network, Toronto, Ontario, Canada
[4]Institute of Medical Science, University of Toronto, Toronto, Ontario, Canada
[5]Princess Margaret Cancer Centre, University Health Network, Toronto, Ontario, Canada
[6]School of Cancer Sciences, University of Glasgow, Glasgow, UK
[7]Department of Medical Parasitology and Infection Biology, Swiss Tropical and Public Health Institute, Allschwil, Switzerland
[8]University of Basel, Basel, Switzerland
[9]Nubiyota LLP, Guelph, Ontario, Canada
[10]University of Guelph, Guelph, Ontario, Canada
[11]Division of Medical Oncology and Hematology, Princess Margaret Cancer Centre, University Health Network, Toronto, Ontario, Canada
[12]Department of Medicine, Division of Infectious Diseases, University of Toronto, Toronto, Ontario, Canada

X Lillian L Siu @lillian_siu

ORCID iDs
Matthew K Wong http://orcid.org/0009-0007-4746-7571
Anna Spreafico http://orcid.org/0000-0002-3034-3042

REFERENCES

1 Li Y, Elmén L, Segota I, *et al*. Prebiotic-Induced Anti-tumor Immunity Attenuates Tumor Growth. *Cell Rep* 2020;30:1753–66.
2 Spencer CN, McQuade JL, Gopalakrishnan V, *et al*. Dietary fiber and probiotics influence the gut microbiome and melanoma immunotherapy response. *Science* 2021;374:1632–40.
3 Zhang S-L, Mao Y-Q, Zhang Z-Y, *et al*. Pectin supplement significantly enhanced the anti-PD-1 efficacy in tumor-bearing mice humanized with gut microbiota from patients with colorectal cancer. *Theranostics* 2021;11:4155–70.
4 Davar D, Dzutsev AK, McCulloch JA, *et al*. Fecal microbiota transplant overcomes resistance to anti-PD-1 therapy in melanoma patients. *Science* 2021;371:595–602.
5 Baruch EN, Youngster I, Ben-Betzalel G, *et al*. Fecal microbiota transplant promotes response in immunotherapy-refractory melanoma patients. *Science* 2021;371:602–9.
6 Tanoue T, Morita S, Plichta DR, *et al*. A defined commensal consortium elicits CD8 T cells and anti-cancer immunity. *Nature New Biol* 2019;565:600–5.
7 Spreafico A, Heirali AA, Araujo DV, *et al*. First-in-class Microbial Ecosystem Therapeutic 4 (MET4) in combination with immune checkpoint inhibitors in patients with advanced solid tumors (MET4-IO trial). *Ann Oncol* 2023;34:520–30.
8 Wong MK, Barbulescu P, Coburn B, *et al*. Therapeutic interventions and mechanisms associated with gut microbiota-mediated modulation of immune checkpoint inhibitor responses. *Microbes Infect* 2021;23:104804.
9 Petrof EO, Claud EC, Gloor GB, *et al*. Microbial ecosystems therapeutics: a new paradigm in medicine? *Benef Microbes* 2013;4:53–65.
10 Vétizou M, Pitt JM, Daillère R, *et al*. Anticancer immunotherapy by CTLA-4 blockade relies on the gut microbiota. *Science* 2015;350:1079–84.
11 Matson V, Fessler J, Bao R, *et al*. The commensal microbiome is associated with anti-PD-1 efficacy in metastatic melanoma patients. *Science* 2018;359:104–8.
12 Routy B, Le Chatelier E, Derosa L, *et al*. Gut microbiome influences efficacy of PD-1-based immunotherapy against epithelial tumors. *Science* 2018;359:91–7.
13 Gopalakrishnan V, Spencer CN, Nezi L, *et al*. Gut microbiome modulates response to anti-PD-1 immunotherapy in melanoma patients. *Science* 2018;359:97–103.
14 Paun A, Yau C, Meshkibaf S, *et al*. Association of HLA-dependent islet autoimmunity with systemic antibody responses to intestinal commensal bacteria in children. *Sci Immunol* 2019;4:eaau8125.
15 Andrews S. FastQC a quality control tool for high throughput sequence data. Babraham Bioinformatics; 2010. Available: https://www.bioinformatics.babraham.ac.uk/projects/fastqc/ [Accessed 11 Mar 2024].
16 Bolger AM, Lohse M, Usadel B. Trimmomatic: a flexible trimmer for Illumina sequence data. *Bioinformatics* 2014;30:2114–20.
17 Huttenhower C. KneadData. The Huttenhower Lab, 2022. Available: https://huttenhower.sph.harvard.edu/kneaddata/ [Accessed 11 Mar 2024].
18 Blanco-Míguez A, Beghini F, Cumbo F, *et al*. Extending and improving metagenomic taxonomic profiling with uncharacterized species using MetaPhlAn 4. *Nat Biotechnol* 2023;41:1633–44.
19 Truong DT, Franzosa EA, Tickle TL, *et al*. MetaPhlAn2 for enhanced metagenomic taxonomic profiling. *Nat Methods* 2015;12:902–3.
20 Tong J, Liu C, Summanen P, *et al*. Application of quantitative real-time PCR for rapid identification of Bacteroides fragilis group and related organisms in human wound samples. *Anaerobe* 2011;17:64–8.

21 Junick J, Blaut M. Quantification of human fecal bifidobacterium species by use of quantitative real-time PCR analysis targeting the groEL gene. *Appl Environ Microbiol* 2012;78:2613–22.

22 Kim S, Shin Y-C, Kim T-Y, *et al*. Mucin degrader Akkermansia muciniphila accelerates intestinal stem cell-mediated epithelial development. *Gut Microbes* 2021;13:1–20.

23 Mohammadi T, Reesink HW, Vandenbroucke-Grauls CMJE, *et al*. Optimization of real-time PCR assay for rapid and sensitive detection of eubacterial 16S ribosomal DNA in platelet concentrates. *J Clin Microbiol* 2003;41:4796–8.

24 Lyra A, Forssten S, Rolny P, *et al*. Comparison of bacterial quantities in left and right colon biopsies and faeces. *World J Gastroenterol* 2012;18:4404–11.

25 Caporaso JG, Lauber CL, Walters WA, *et al*. Ultra-high-throughput microbial community analysis on the Illumina HiSeq and MiSeq platforms. *ISME J* 2012;6:1621–4.

26 Bolyen E, Rideout JR, Dillon MR, *et al*. Reproducible, interactive, scalable and extensible microbiome data science using QIIME 2. *Nat Biotechnol* 2019;37:852–7.

27 Ewels P, Magnusson M, Lundin S, *et al*. MultiQC: summarize analysis results for multiple tools and samples in a single report. *Bioinformatics* 2016;32:3047–8.

28 Martin M. Cutadapt removes adapter sequences from high-throughput sequencing reads. *EMBnet j* 2011;17:10.

29 Edgar RC. Search and clustering orders of magnitude faster than BLAST. *Bioinformatics* 2010;26:2460–1.

30 Rognes T, Flouri T, Nichols B, *et al*. VSEARCH: a versatile open source tool for metagenomics. *PeerJ* 2016;4:e2584.

31 Bokulich NA, Kaehler BD, Rideout JR, *et al*. Optimizing taxonomic classification of marker-gene amplicon sequences with QIIME 2's q2-feature-classifier plugin. *Microbiome* 2018;6:90.

32 Kaehler BD, Bokulich NA, McDonald D, *et al*. Species abundance information improves sequence taxonomy classification accuracy. *Nat Commun* 2019;10:4643.

33 Janssen S, McDonald D, Gonzalez A, *et al*. Phylogenetic Placement of Exact Amplicon Sequences Improves Associations with Clinical Information. *mSystems* 2018;3:e00021-18.

34 Davis NM, Proctor DM, Holmes SP, *et al*. Simple statistical identification and removal of contaminant sequences in marker-gene and metagenomics data. *Microbiome* 2018;6:226.

35 Mallick H, Rahnavard A, McIver LJ, *et al*. Multivariable association discovery in population-scale meta-omics studies. *PLoS Comput Biol* 2021;17:e1009442.

36 Gadalla R, Boukhaled GM, Brooks DG, *et al*. Mass cytometry immunostaining protocol for multiplexing clinical samples. *STAR Protoc* 2022;3:101643.

37 Zeng MY, Cisalpino D, Varadarajan S, *et al*. Gut Microbiota-Induced Immunoglobulin G Controls Systemic Infection by Symbiotic Bacteria and Pathogens. *Immunity* 2016;44:647–58.

38 Routy B, Lenehan JG, Miller WH Jr, *et al*. Fecal microbiota transplantation plus anti-PD-1 immunotherapy in advanced melanoma: a phase I trial. *Nat Med* 2023;29:2121–32.

39 Ciccarese C, Porcari S, Buti S, *et al*. LBA77 Fecal microbiota transplantation (FMT) versus placebo in patients receiving pembrolizumab plus axitinib for metastatic renal cell carcinoma: Preliminary results of the randomized phase II TACITO trial. *Ann Oncol* 2024;35:S1264.

40 Vujkovic-Cvijin I, Welles HC, Ha CWY, *et al*. The systemic anti-microbiota IgG repertoire can identify gut bacteria that translocate across gut barrier surfaces. *Sci Transl Med* 2022;14:3927.

41 Paston SJ, Brentville VA, Symonds P, *et al*. Cancer Vaccines, Adjuvants, and Delivery Systems. *Front Immunol* 2021;12:627932.

42 Duan T, Du Y, Xing C, *et al*. Toll-Like Receptor Signaling and Its Role in Cell-Mediated Immunity. *Front Immunol* 2022;13:812774.

43 Griffin ME, Espinosa J, Becker JL, *et al*. *Enterococcus* peptidoglycan remodeling promotes checkpoint inhibitor cancer immunotherapy. *Science* 2021;373:1040–6.

44 Kim CH. Control of lymphocyte functions by gut microbiota-derived short-chain fatty acids. *Cell Mol Immunol* 2021;18:1161–71.

45 Kolypetri P, Weiner HL. Monocyte regulation by gut microbial signals. *Trends Microbiol* 2023;31:1044–57.